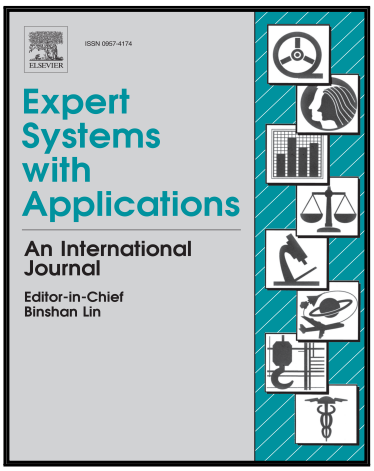

Automatic Abdominal Aortic Aneurysm Segmentation in MR Images

Sergio Martinez-Muñoz , Daniel Ruiz-Fernandez ,
Juan Jose Galiana-Merino

PII: S0957-4174(16)00027-0
DOI: 10.1016/j.eswa.2016.01.017
Reference: ESWA 10468

To appear in: *Expert Systems With Applications*

Received date: 19 November 2014
Revised date: 11 January 2016
Accepted date: 12 January 2016

Please cite this article as: Sergio Martinez-Muñoz , Daniel Ruiz-Fernandez , Juan Jose Galiana-Merino , Automatic Abdominal Aortic Aneurysm Segmentation in MR Images, *Expert Systems With Applications* (2016), doi: 10.1016/j.eswa.2016.01.017

Highlights

- We use a spatial fuzzy C-means algorithm to detect and segment the lumen
- We use a graph cut algorithm to segment the aortic wall
- The detection and segmentation process is fully automatic
- We get a 79% overlapping between our segmentation and the one from the specialist

Automatic Abdominal Aortic Aneurysm Segmentation in MR Images

Sergio Martinez-Muñoz[(1)], Daniel Ruiz-Fernandez[(1,2,*)], Juan Jose Galiana-Merino[(3, 4)]

[(1)] IBIS Research Group, University of Alicante, P.O.Box 99, E-03080 Alicante, Spain

[(2)] Dept. Computing Technology and Data Processing, University of Alicante, P.O.Box 99, E-03080 Alicante, Spain

[(3)] University Institute of Physics Applied to Sciences and Technologies University of Alicante, Spain

[(4)] Dept. Physics, Systems Engineering and Signal Theory, University of Alicante, P.O.Box 99, E-03080 Alicante, Spain

E-mail: smartinez@ibisrg.com , druiz@dtic.ua.es, juanjo@dfists.ua.es

*Corresponding author: Daniel Ruiz-Fernandez

Abstract

Abdominal Aortic Aneurism is a disease related to a weakening in the aortic wall that can cause a break in the aorta and the death. The detection of an unusual dilatation of a section of the aorta is an indicative of this disease. However, it is difficult to diagnose because it is necessary image diagnosis using computed tomography or magnetic resonance. An automatic diagnosis system would allow to analyze abdominal magnetic resonance images and to warn doctors if any anomaly is detected. We focus our research in magnetic resonance images because of the absence of ionizing radiation. Although there are proposals to identify this disease in magnetic resonance images, they need an intervention from clinicians to be precise and some of them are computationally hard. In this paper we develop a novel approach to analyze magnetic resonance abdominal images and detect the lumen and the aortic wall. The method combines different algorithms in two stages to improve the detection and the segmentation so it can be applied to similar problems with other type of images or structures. In a first stage, we use a spatial fuzzy C-means algorithm with morphological image analysis to detect and segment the lumen; and subsequently, in a second stage, we apply a graph cut algorithm to segment the aortic wall. The obtained results in the analyzed images are pretty successful obtaining an average of 79% of overlapping between the automatic segmentation provided by our method and the aortic wall identified by a medical specialist. The main impact of the proposed method is that it works in a completely automatic way with a low computational cost, which is of great significance for any expert and intelligent system.

Index Terms – Abdominal Aortic Aneurism, image segmentation, spatial fuzzy C-means, Graph cut, morphological analysis

1. Introduction

Abdominal Aortic Aneurysm (AAA) is a disease caused by a weakening in the aortic wall that leads to an abnormal dilation of the aorta. Probability of vessel rupture increases with the size of the aneurysm. Maximum diameter of the aorta is the key parameter in AAA diagnosis: a diameter of 30 mm is typically considered as the threshold to define an AAA, meanwhile a value of 55 mm means that the risk of rupture increases exponentially and surgical intervention is recommended (Hutchison, 2009).

Typical imaging techniques are ultrasonography, computed tomography (CT) and magnetic resonance (MR). The first one is used for general AAA screening but lacks the precision of the other imaging methods. Therefore, CT and MR imaging techniques are used for an accurate diagnosis (Isselbacher, 2005). MR imaging has some advantages over CT scans: absence of ionizing radiation; better soft tissue contrast (Haulon et al., 2001); and it is also not affected by calcifications. Besides, it is the only imaging technique in which the aortic wall surrounding the thrombus is visible.

Normally, aneurysms must be identified and segmented manually by a radiologist, which is a time-consuming and cumbersome task (Macia et al., 2009). A common approach in computer-assisted methods is to segment aortic wall and lumen from individual CT or MR images (Kronman and Joskowicz, 2015; Maiora et al., 2014; Zohios et al., 2012). A 3D reconstruction of the artery could then be performed using the boundaries obtained (Kim et al., 2010; Shim et al., 2009). Other methods perform a full 3D segmentation in one single step, profiting from the usage of more information simultaneously (Ayyalasomayajula et al., 2010; Lee et al., 2010). It should also be noted that 4D methods (3D throughout the cardiac cycle) have been also proposed (Hameeteman et al., 2013; Zhao et al., 2009).

In order to analyze this kind of information (2D, 3D CT or MR images) in a fast

and effective way, automatic or semi-automatic computer-assisted segmentation methods become crucial for the diagnosis of AAA (Shang et al., 2015). Thus, many different algorithms have been adopted to achieve semi-automatic aortic segmentation. Methods based on region growing (Borghi et al., 2006), watershed (Lopez-Mir et al., 2011) or, especially, active contour (also called snakes) algorithms (Kass et al., 1988; Loncaric et al., 2000) have been proposed. However, these methods rely solely on intensity information in abdominal MR images, which is an error-prone characteristic as other structures with similar intensity levels may appear adjacent to the aorta. This may cause leaks in the segmented contour. These methods also require an accurate initialization process, which has to be done manually to achieve good results. Although several variations of snakes have been developed in order to minimize instability (Xu and Prince, 1998) or ease initialization restraints (Tauber et al., 2010), snakes-based methods are computationally costly due to the use of differential equations and still require a clear differentiation of aortic structures to obtain good results.

A solution is to combine intensity information with shape models. This approach has been adopted by level-set methods (Nakhjavanlo et al., 2011; Subasic et al., 2005; Zohios et al., 2012) with good results. However, level-sets are computationally demanding and hard to implement, besides of needing a previous knowledge of the aortic shape to segment. This is difficult to predict in the case of a diseased aorta and often translates into a time-consuming manual initialization.

In the research for fully automatic AAA segmentation, several methods based on fuzzy clustering have been proposed (Majd et al., 2010; Pham and Golledge, 2008). In (Majd et al., 2010) a Fuzzy C-Means (FCM) clustering technique that incorporates spatial properties named Spatial-FCM (SFCM) (Ahmed et al., 1999; Chuang et al., 2006) is applied to AAA segmentation. With the appropriate use of morphological

operations this method can achieve automatic segmentation of the aortic thrombus. Unfortunately, it is only suitable for CT images, since it does not provide good results with abdominal MR imaging.

Another alternative is graph cut algorithms (Boykov et al., 2001; Boykov and Jolly, 2001). Several methods for abdominal aortic segmentation using graph cuts have been proposed (Duquette et al., 2012; Freiman et al., 2010). The method proposed in (Duquette et al., 2012) is able to perform segmentation in MR images in addition to CT ones. However, despite being a method able to segment the lumen and aortic wall in a faster and more computationally efficient way in MR images, it needs an accurate manual initialization in order to work properly.

Thus, the main drawbacks detected in the previously commented algorithms can be summarized in the following points: non-completely automatic algorithms (most of them need the expert assistance to select the area of analysis); high-computational demand; or poor results when they are applied on MR images. Therefore it is clear that there is not a single method that can perform automatic AAA segmentation from MR images efficiently.

In this work we have developed a new approach that intends to surpass all these inconveniences, providing a complete automatic and low computational cost program that works properly with MR images. For that, the proposed scheme uses a combination of different techniques, profiting from their respective advantages and minimizing the corresponding drawbacks.

Thus, in this paper we propose specifically a mixed method for automatic AAA segmentation in MR images. Our method uses the SFCM algorithm to detect and segment the aortic lumen in a first stage, following with the thrombus and aortic wall segmentation via graph cuts. We use the results of the first stage (lumen segmentation)

to improve the segmentation of the aortic wall in the second stage. In this way, we avoid manual or expert help in the second stage to maximize the results of graphs cut algorithm. The proposed approach is fully automatic, computationally efficient and works in MR images. The use of a mixed method is a novel approach and could open new possibilities in this field.

2. Methodology

The proposed method is divided basically in two different stages to achieve the automatic AAA segmentation, as it is shown in Fig. 1.

Previously to these stages, the acquired MR image is pre-processed using a low-pass Wiener filter to eliminate possible noise contamination and windowed to select the central region of interest in which the aorta appears in axial abdominal imaging.

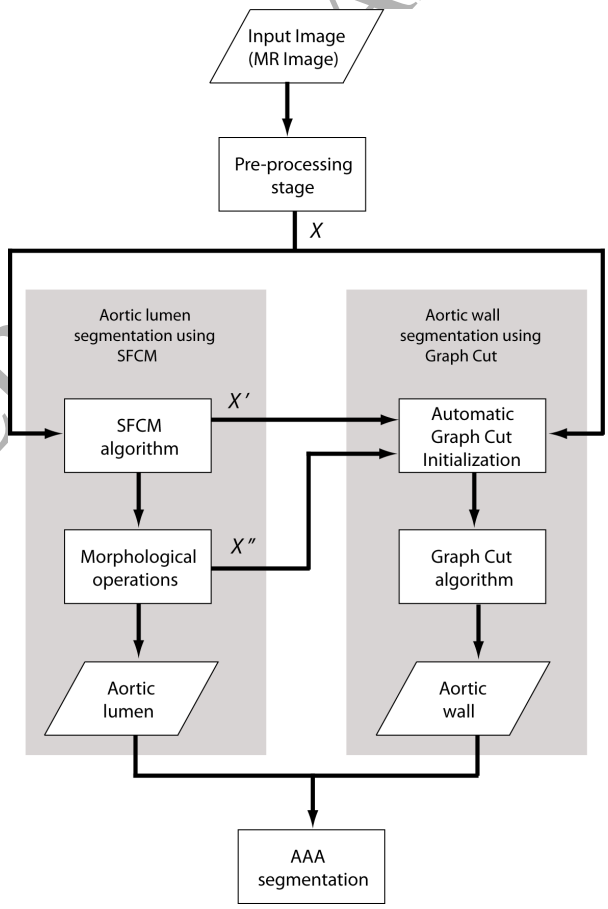

Fig. 1. Flow chart of the proposed method.

Once the MR image has been pre-processed, the first processing stage provides the aortic lumen segmentation using the SFCM algorithm and morphological operations.

The second stage of the proposed method achieves the thrombus and aortic wall segmentation using graph cuts. To solve the problem of the manual initialization required by the graph cut to work correctly, an automatic initialization approach has been developed using the results previously obtained from the SFCM algorithm.

In the following sections, we describe in detail the different stages of the developed method.

2.1 Lumen segmentation

The lumen segmentation process was inspired by the method proposed in (Majd et al., 2010). The original method achieves automatic segmentation of aortic lumen and thrombus in CT scans, but this is not applicable to MR images, where the background and surrounding tissues can be brighter than the thrombus and the aortic wall. Therefore, in the proposed method, we have adapted the original SFCM algorithm in order to carry out also the lumen segmentation in MR images.

2.1.1. Spatial Fuzzy C-Means (SFCM) algorithm

The FCM algorithm classifies an image by grouping similar pixels in the feature space into clusters. This clustering is achieved by iteratively minimizing a cost function that is dependent on the distance of the pixels to the cluster centers in the feature domain.

Let $X=(x_1, x_2, \ldots, x_N)$ be a gray-scale image of N pixels, where x_i represents the feature set of a pixel i. In our case, this feature set is reduced just to the intensity parameter. Then, our first objective consists in identifying the parts of the image that might pertain to the lumen, which implies to divide the image in two different clusters,

depending on their possibility of belonging or not to the lumen based on their intensity level.

The SFCM follows an iterative optimizing process whose aim is to minimize a cost function defined as:

$$J = \sum_{j=1}^{N} \sum_{i=1}^{n^o of\ clusters} \left(u_{ij}\right)^m \cdot \left(x_j - v_i\right)^2 \tag{1}$$

where u_{ij} is the membership matrix that represents the probability (between 0 and 1) of pixel j to belong to the cluster ith; v_i is the ith cluster center; and m is a constant that regulates the fuzziness of the membership. The higher the membership values assigned to pixels close to their cluster centers, the lower the cost function will be.

Once an initial value is randomly assigned for each cluster center, the iterative process is carried out through the following steps:

Step 1. Estimation of the membership matrix in the feature domain

$$u_{ij} = \frac{1}{\sum_{k=1}^{n^o of\ clusters} \left(\frac{x_j - v_i}{x_j - v_k} \right)^{\frac{2}{m-1}}} \tag{2}$$

Step 2. Estimation of a spatial function, defined as:

$$h_{ij} = \sum_{k \in NB(x_j)} u_{ik} \tag{3}$$

where $NB(x_j)$ is a square window centered on pixel j in the spatial domain. In our case, a 5x5 window has been selected. The higher the number of neighborhood pixels that belong to the same cluster than the central pixel, the higher the spatial function value for this central pixel.

Step 3. Incorporation of the spatial function into the membership function

$$u'_{ij} = \frac{u_{ij}^{p} \cdot h_{ij}^{q}}{\sum_{k=1}^{n^o of\ clusters} u_{kj}^{p} \cdot h_{kj}^{q}} \tag{4}$$

where p and q are constants used to weight both functions.

Step 4. Update the cluster center values

$$v_i = \frac{\sum_{j=1}^{N} \left(u'_{ij}\right)^m \cdot x_j}{\sum_{j=1}^{N} \left(u'_{ij}\right)^m} \tag{5}$$

The iteration stops when the maximum difference between the cluster centers at two successive iterations is lower than a pre-defined threshold value. In our case, this threshold value has been set up to 0.01. Moreover, we have limited the number of iterations in order to avoid unnecessary slowness or even non-convergent solutions that might cause infinite loops. Nevertheless, the defined upper limit (200 iterations) has been never reached in the analyzed test cases.

Once a solution has been reached, a binarization threshold is applied to the brightest cluster in the membership matrix u_{ij}. The brightest cluster is determined by the highest intensity cluster center v_i. In our method, the binarization threshold has been fixed at 99% of the membership probability. The thresholded resulting image, called X' (Fig. 2b), will be used to extract the lumen through morphological operations as well as generate an automated initialization for the graph cut used subsequently in the aortic wall segmentation stage.

2.1.2. Lumen extraction through morphological operations

After applying the SFCM algorithm, our method extracts automatically the lumen from the resulting binarized image using morphological operations, as it is shown

in Fig. 2. To successfully identify and segment the lumen, its known properties must be exploited. These recognizable properties are the following:

1) The lumen is roughly found in the central part of the image. This is due to the abdominal anatomical structure.

2) Though it is difficult to predict the shape of a diseased aorta due to the possible presence of a thrombus, the lumen can be modeled approximately as a circular shape object.

3) It appears as a relatively big object among the resulting binary objects obtained after the SFCM processing stage.

Therefore, the morphological method proposed for the lumen extraction is directed by location, shape and size guidelines. The first step to achieve the segmentation of the lumen is to remove binary objects touching the image border in order to consider only objects fully contained inside the region of interest. To do that we use an algorithm proposed by (Soille, 1999) based on the neighborhood of the border pixels. We apply an 8-connectivity, so that, we decide that a pixel is touching the border when one of its 8 neighbors belongs to the border.

After that, a morphological reconstruction of those objects is then performed with the purpose of filling holes inside their boundaries. We implement two morphological operations to do this reconstruction. First, we bridge unconnected pixels in the following way: if a pixel (0-valued) has two non-zero neighbors (which are not connected), we set that pixel to 1. The second morphological operation consists in filling the ‘holes’ in the image. In our context, a ‘hole’ is a set of pixels (0-valued) that cannot be reached (with 4-connectivity) from the edge of the image, so they do not belong to the image background. When a ‘hole’ is identified, its pixels are set to 1 according to a 4-connectivity.

Next, we label the remaining objects in the image to calculate their shape and size using a 4-connectivity algorithm. To evaluate the shape of the objects, it is calculated a circularity parameter, *C*, that relates the corresponding area, *A*, and perimeter, *P*.

$$C = \frac{P^2}{4 \cdot \pi \cdot A} \tag{6}$$

This parameter ranges from 1 in the case of a perfect circle to higher values in cases were the shape is deformed and its perimeter is larger than the expected area for a circle. It should be noted that measuring shape perimeters in digital images can be error-prone and yield unexpected results in small-sized objects. Fortunately, this corruption tends to be minimized in bodies of larger size and therefore does not affect the lumen extraction.

The lumen identification is completed incorporating the information about the size of the objects. Using the calculated circularity parameter and the area of the object, we have defined a lumen factor, *L*, defined as the relationship between the area and the circularity:

$$L = \frac{A^r}{C^s} \tag{7}$$

where *r* and *s* are weighting exponents for the area and circularity of the object. Experimentally, we have obtained the best results when *r* and *s* have a similar order of magnitude.

The lumen factor is calculated for every object in the image. Objects closer to the lumen in size and shape will attain larger *L* values. Thus, the binary body with the largest lumen factor will be selected and identified as the lumen. After that, the rest of objects are set up to 0, providing a new binary image, *X*'' (Fig. 2e), with only one object, the lumen.

Fig. 2 shows the whole process of the lumen segmentation through the SFCM algorithm and the morphological operations. In Fig. 2f we present the final graphical interpretation of the results applied to the original image, showing the contour of the segmented lumen over the input image.

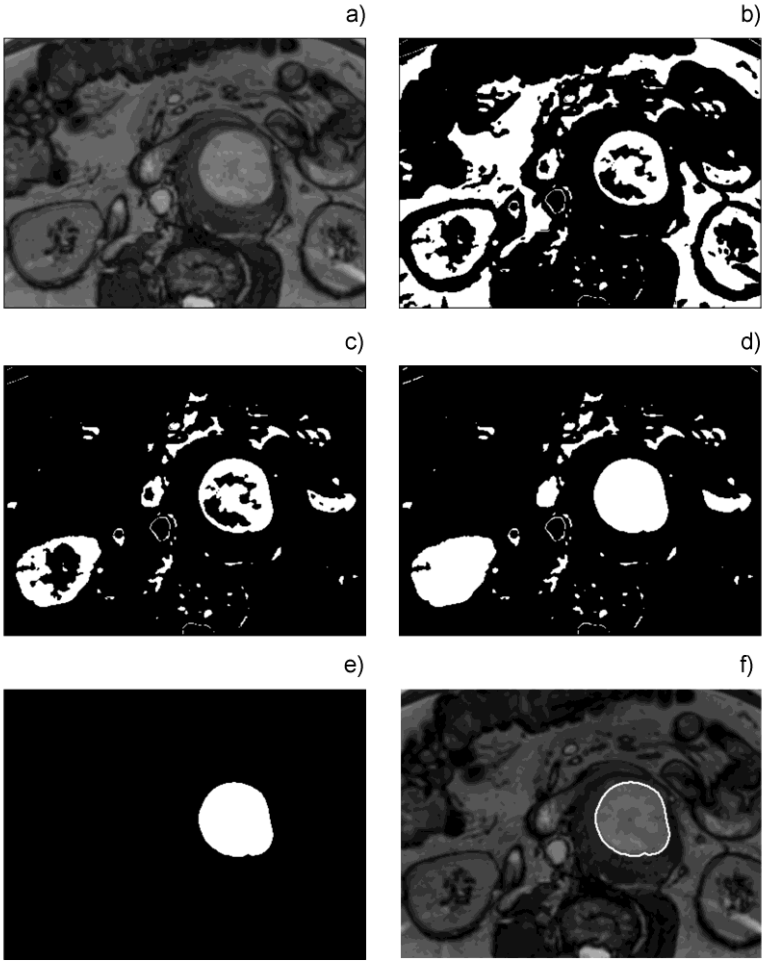

Fig. 2. Graphical description of the lumen extraction process. (a) Input image. (b) Thresholded SFCM results. (c) Removal of objects touching the edge of the image. (d) Morphological reconstruction. (e) Selection of the object with the highest lumen factor, *L*. (f) Final result of the lumen segmentation stage.

2.2 Thrombus and aortic wall segmentation

In the second stage of the proposed method both aortic wall and thrombus (in case it exists) are segmented in a single step. The method aims for the identification and

segmentation of the outer aortic wall boundary, automatically classifying the region inside the generated contour as part of the aortic wall or thrombus.

2.2.1 Graph cut algorithm

Graph cuts are algorithms whose purpose is to divide an image (interpreted as a graph) in different regions, in such a way that the cut between the regions achieves an optimal minimum cost. The cost function is defined according to the application, modifying the behavior of the algorithm. This is the reason why graph cuts are regarded as very versatile methods.

In our case, the image is initially divided into 3 regions: the "object" region ("*obj*"), the "background" region ("*bkg*") and the undefined region, where the optimal cut is computed. At the end of the process, the pixels belonging to the undefined region will be assigned to the "*obj*" or "*bkg*" regions.

For that, let's consider the original gray-scale image $X=(x_1, x_2, \ldots, x_N)$ of N pixels, where x_i represents the intensity. In this case, the associated graph is formed by N nodes, corresponding to each pixel of the image, plus two terminal nodes, called source (S) and sink (T) nodes, which are related with the "*obj*" and "*bkg*" regions, respectively. Each node at position i in the image is connected to its 4 neighbors, i.e. the pixels located in the up-down and right-left directions. In this way, a 4-neighborhood system that connects each pair of neighboring pixels, i and j, is configured in a set of non-directed edges, ε. These neighborhood edges or links, represented as $\{i, j\}$, are called n-links and each one of them, $\{i, j\} \in \varepsilon$, is assigned a non-negative weight or cost, $w_{\{i,j\}}$. Besides, each pixel has also two additional links connecting with the terminal nodes, which are called t-links. In this case, the cost assigned to these t-links is a constant value, K, (or zero) depending on the belonging (or not) to the respective regions ("obj" and "bkg") associated with the terminal nodes, S and T. For the

undefined pixels, the cost of both *t*-links remains zero to allow the *n*-links to be the driving factor in the segmentation process. The constant value, *K*, has to be large enough to surpass the sum of all the *n*-link costs, which assures the connection to the respective region. In our case, it is enough to choose a *K* higher than 4.

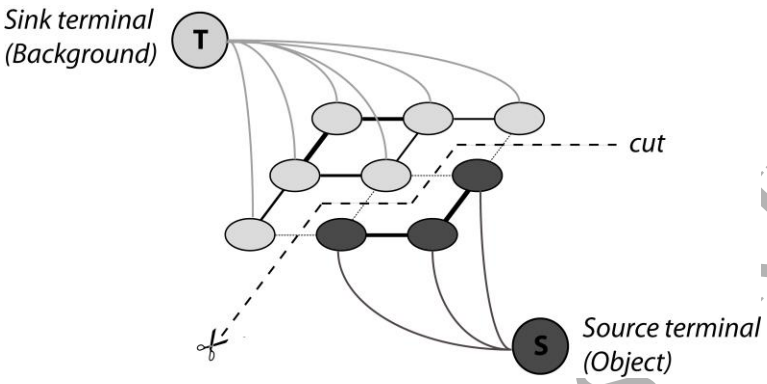

Fig. 3. Example of a 2D segmentation for a 3x3 image using the graph cut algorithm. The object nodes, associated with the source terminal, and the background nodes, associated with the sink terminal, are represented by dark and light gray circles, respectively. The cost of each edge is reflected by the edge's thickness. The calculated cut between regions (dashed line) and the severed links (dotted lines) are also shown.

In this context, a cut is defined as a subset of edges $E \subset \varepsilon$ such that the graph is divided in two sets of nodes, belonging univocally to one of the "*obj*" or "*bkg*" regions, The cost of a given cut, *E*, is expressed as the sum of the weights of the edges that were cut:

$$\cos t\{E\} = \sum_{\{i,j\} \in E} w_{\{i,j\}} \tag{8}$$

The objective of the graph cut algorithm is to find a cut with the minimum cost, which means to sever the edges with the lower weights (represented by the thinnest lines in Fig. 3) and leave the strongest links untouched.

Respecting to the cost function, $w_{\{i,j\}}$, we propose a modified version of the

expression given by (Duquette et al., 2012) in order to carry out the image segmentation in the outer boundary of the aortic wall. The objective is to define an expression that attracts the cut to such areas. In abdominal MR images the aortic wall appears as a thin and dark object surrounding the aorta. As the totality of the aortic wall has to be inside the segmented contour, the cost function used has to attract the cut to sharp intensity gradients whose transition happens from darker to brighter pixels (measured from the center of the aorta) as is the case at the outer boundary of the aortic wall. Therefore, attending to these considerations, the proposed cost function is defined as:

$$w_{\{i,j\}} = \exp\left(-\frac{\delta_{i,j} \cdot \left|x_i - x_j\right|^{\gamma} \cdot \mu_{i,j}^{\rho}}{2\sigma^2}\right) \tag{9}$$

where $\left|x_i - x_j\right|$ is the intensity gradient between the pixels *i* and *j*; $\delta_{i,j}$ is a binary function that controls the direction of the intensity gradient; $\mu_{i,j}$ is an intensity-based parameter that attracts the cut to low intensity areas; σ is a "camera noise" factor; and both γ and ρ are weighting exponents for the intensity gradient and the intensity-based parameter, respectively. We can observe that $w_{\{i,j\}}$ will take values comprised between 0 and 1. Higher values of the exponent grant lower weight costs. Therefore, sharpest intensity gradients attract the cut towards these edges.

The binary function, $\delta_{i,j}$, is defined as:

$$\delta_{i,j} = \begin{cases} 1 & if\ \left(d_i < d_j\ and\ x_i < x_j\right) or\ \left(d_i > d_j\ and\ x_i > x_j\right) \\ 0 & otherwise \end{cases} \tag{10}$$

where d_i (and d_j) is the Euclidean distance from the center of the aorta to the pixel *i* (or *j*). The $\delta_{i,j}$ parameter guarantees that the transition at the segmented contour is correct. In an abdominal MR image, the darker aortic wall is surrounded by brighter organs and tissues outside the aorta. Using this parameter only the gradients flowing

from a darker to a brighter pixel (from the center of the aorta) are allowed.

To solve the problem of dealing with an initial broad undefined region, an intensity-based parameter, $\mu_{i,j}$, has been considered to attract the cut to the darker areas such as the aortic wall. The proposed $\mu_{i,j}$ is defined as:

$$\mu_{i,j} = \ln\left(\frac{1}{\left\|CH_X\right\|}\right)\Bigg|_{x_n} \tag{11}$$

where $\left\|CH_X\right\|$ is the cumulative histogram of the input image, X, normalized to 1. The purpose of the logarithm is to reduce the range of the obtained results, avoiding excessively high values for low intensities. The function is then evaluated for an intensity level x_n, which is determined as:

$$x_n = \begin{cases} x_i & if \quad A_{Lumen} > 0.02 \cdot A_X \quad and \quad d_i < d_j \\ x_j & if \quad A_{Lumen} > 0.02 \cdot A_X \quad and \quad d_i > d_j \\ \dfrac{x_i + x_j}{2} & if \quad A_{Lumen} < 0.02 \cdot A_X \end{cases} \tag{12}$$

where A_{Lumen} and A_X are the areas of the lumen (obtained previously in section 2.1) and the original image, respectively.

In images where the lumen is smaller, we have found experimentally that better results are achieved if the intensity level, x_n, used to evaluate the expression in (11) is the average between the two pixels of the link, i.e. the pixels i and j. The use of the average intensity steadies the cut and prevents it from snapping other objects that may fall inside the undefined region. However, in images where the lumen is larger, the probability of other objects falling into the undefined region (in its entirety) is lower and is preferable to sharpen the cut by using the intensity of the nearest pixel. The limit for the use of the average intensities was set at lumen areas smaller than 2% of the total

input image.

In Fig. 4, we show the $\mu_{i,j}$ values estimated for all the input intensities, x_n, registered during the segmentation of the aortic wall in one of our test images. We have highlighted the range of intensities reinforced by this parameter, i.e. $\mu_{i,j} > 1$. For this particular image the aortic wall was found in the intensity range between 10 and 30. Thus, in each analyzed image, the range of intensities at which the aortic wall is located is reinforced by this parameter.

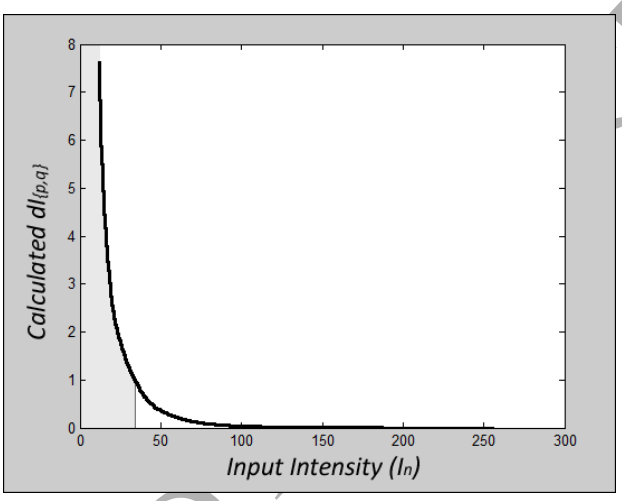

Fig. 4. $\mu_{i,j}$ values assigned to an input x_n. Values reinforced by the $\mu_{i,j}$ parameter ($\mu_{i,j}$>1) are highlighted.

In Fig. 5, we show the effect of the intensity-based parameter, $\mu_{i,j}$, in a synthetic test image. Fig. 5a shows an image simulating the conditions of an abdominal MR image containing a diseased aorta. The circular bright object in the middle (label 1) represents the lumen. The dark line around the lumen (label 2) simulates the aortic wall. The grey area caught between these objects (label 3) is the aortic thrombus, while the part outside the aortic wall represents outer tissues and organs adjacent to the aorta (label 4). The brighter exterior area (label 5) represents brighter tissues that are far from the aorta.

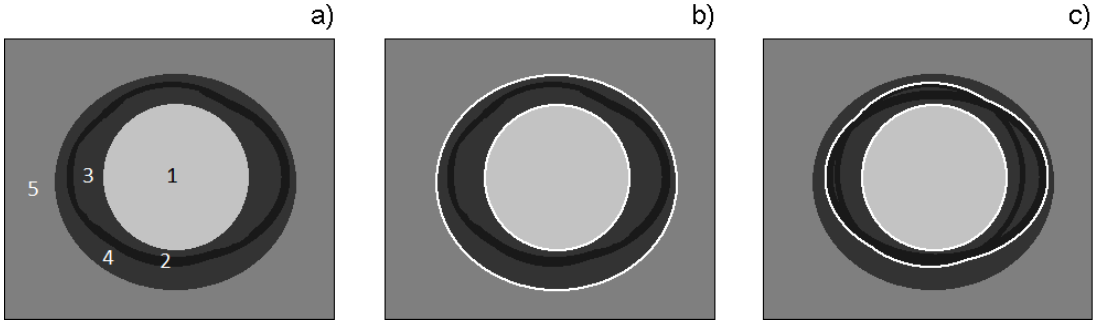

Fig. 5. Effect of $\mu_{i,j}$ on a synthetic image: (a) Original image; (b) segmentation without the $\mu_{i,j}$ parameter; (c) segmentation using the $\mu_{i,j}$ parameter.

Using an automatic initialization, the undefined region where the cut is performed, often includes a wide variety of objects that can mislead the cut if there are larger gradients than the one found in the aortic wall. To test this situation we added a bright area (assigned to label 5) that creates a large intensity gradient between the zones labeled as 4 and 5. This gradient is larger than the one found in the aortic wall between the areas labeled as 3 and 4.

In Fig. 5b, we show the results of applying the graph cut algorithm following the cost function indicated in (Boykov and Jolly, 2001) , i.e. without including the $\mu_{i,j}$ parameter in equation 9. In this case the cut is performed at the sharpest gradient, effectively ignoring the aortic wall. In contrast, when the $\mu_{i,j}$ parameter is included, the correct result is obtained (see Fig. 5c). In this case, the cut behavior is modified by the new intensity constraint, being more attracted to gradients in dark objects, as is the case of the aortic wall.

To control the relative importance of the intensity gradient, $|x_i - x_j|$, and the intensity-based parameter, $\mu_{i,j}$, two weighting exponents (γ and ρ, respectively) have been included in equation 9. Experimentally, we have achieved better results in

abdominal aortic MR imaging segmentation when both factors are balanced in the equation. Thus, we have used a default value of 2 for both γ and ρ in our tests.

Finally, the "camera noise" factor regulates the influence of both intensity parameters. If $\left|x_i - x_j\right|^{\gamma} \cdot \mu_{i,j}^{\rho} < 2\sigma^2$, then the obtained weight values will be lower than 1 and the cut will be attracted towards the associated edge. Otherwise, the edge will be penalized by a high weight value, being avoided by the cut. For the analyzed images, σ has been set up to 2 by default, which experimentally provides the best results for all the tested cases.

2.2.2 Automatic graph cut initialization

As it was commented in the previous section, before applying the graph cut algorithm to the input image, a first initialization is required in order to classify the pixels as belonging to the "*obj*", the "*bkg*" and the undefined regions. For AAA segmentation in MR images, this initial assignment is usually done manually by the user (e.g. (Duquette et al., 2012)).

In this work, we propose an automatic initialization based on the images obtained from the lumen detection stage. Concretely, we use the image resulting from the SFCM method, *X*', and the binary image with the segmented lumen, *X*''. Both input images are shown in Fig. 6 together with the original MR image.

The goal is to set an area contained inside the aorta as the "*obj*" (connected to the *S* node) and another area with certainty that does not include aortic structures as the "*bkg*" (connected to the *T* node). The unassigned area is then defined as the undefined region where the aortic wall is located and the cut is performed.

Fig. 6. Input arguments of the graph cut initialization: (a) Original image; (b) results of the SFCM algorithm, X'; (c) binary object of the segmented lumen, X''.

The segmented lumen (Fig. 6c) is positively located inside the aortic boundaries and is used in our method to define the "*obj*" region of the graph cut. The results of the SFCM algorithm (Fig. 6b) provide much information about outer aortic structures. However some of the brighter areas of the aortic thrombus may appear in this image and thus is not completely reliable.

Our approach estimates an undefined area around the lumen and tag the rest of the image as the "*bkg*" region. For that, the area where the lumen is contained in the SFCM results image, *X*', is first defined as a starting point. Subsequently, this area is expanded using the bigger objects surrounding the lumen area as the limit for the undefined region. Although other small objects might appear in the thrombus region, only the bigger ones are susceptible to belong to outer aortic structures. The final step is to remove the lumen from the generated expanded area. Next, we describe the different steps of the proposed process:

Step 1. The lumen object (image *X*'') is removed from the SFCM image (*X*') using the "AND" and "NOT" logical operations (Fig. 7a).

Step 2. Small objects are removed (Fig. 7b). We define a "small object" as any binary object whose area is less than a tenth of the lumen area, A_{Lumen}.

Step 3. Convolution between the inverse of the image obtained in the second

step and the lumen (image *X*'') is performed (Fig. 7c).

Step 4. Binary thresholding is applied to select only pixels with the maximum convolution value (Fig. 7d). This represents the areas where the lumen could fit completely into the background image obtained in step 2.

Step 5. The binary object that represents the area where the lumen is located is selected (Fig. 7e). To determine the correct object the centroid of the lumen is used.

Step 6. Convolution of the object obtained in step 5 and the lumen is applied. (Fig. 7f). This step expands the object up to the objects that appeared in step 2 and successfully expands the lumen area to occupy the background that surrounds it.

Step 7. The lumen is subtracted from the image obtained in step 6 to define the undefined region (Fig. 7g). The rest of the image (beyond this area) is defined as the "*bkg*" region, meanwhile the lumen remains as the object ("*obj*" region).

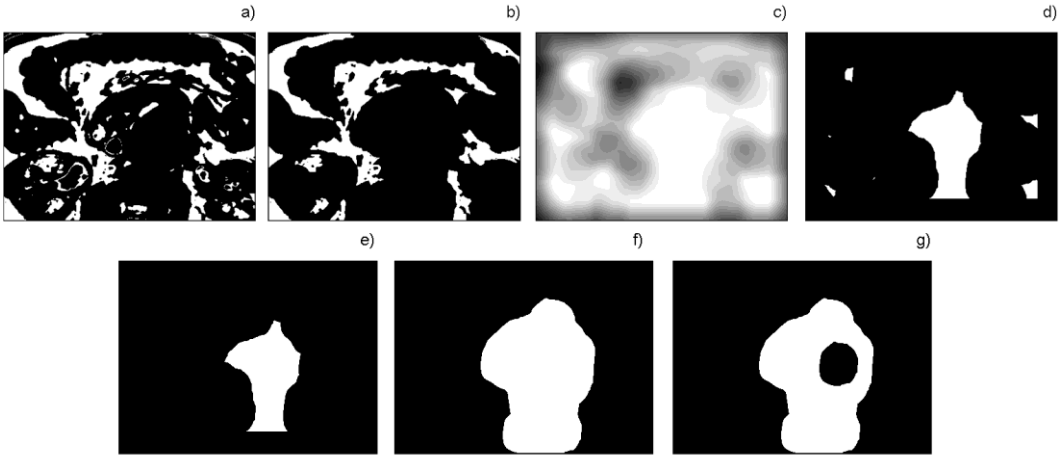

Fig. 7. Graphical example of the graph cut initialization through morphological operations. (a) Removal of the lumen from the SFCM results image; (b) removal of small objects; (c) convolution of the inverse of the previous image and the lumen; (d) binary thresholding, i.e. selection of the maximum values; (e) selection of the area where the lumen is included using the lumen centroid; (f) boolean convolution with the lumen; (g) subtraction of the lumen.

In Fig. 8, we show the three estimated regions marked on the initial image, *X*:

the "*obj*" region (marked with a grid pattern) that corresponds to the lumen; the undefined region (without any mark) where the optimal cut is calculated; and the "*bkg*" region (marked with diagonal lines). In all the analyzed images, we have tested that the undefined region estimated by the proposed method always includes the complete aortic wall.

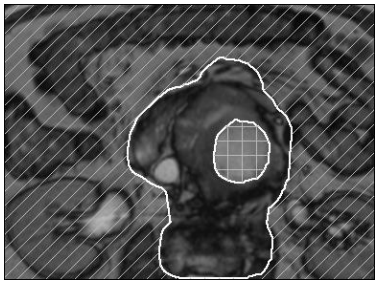

Fig. 8. Interpretation of the automatic initialization generated for the graph cut algorithm: Object region (grid pattern); background region (without any mark); and undefined region (diagonal lines pattern).

3. Results

3.1 Materials

The proposed method has been implemented, tested and validated using MATLAB (Version 7.12.0, R2011a). For the aortic wall segmentation through graph cuts we used the C++ implementation of the Min-Cut/Max-Flow algorithm proposed in (Boykov and Kolmogorov, 2004). We tested the method on a set of abdominal MR images from 8 different patients with different degrees of diseased aortas. To evaluate the performance of the proposed method, the results obtained by the segmentation of the lumen and the aortic wall were compared with the ones validated by an expert.

The proposed method was tested using an Intel Core i7 processor with 4 GB of RAM running on the 64-bit version of Windows 7. The method proved to be very fast: the average time required for the method to automatically segment the lumen through SFCM was 0.91 seconds while the aortic wall segmentation using graph cuts took an

average of 1.90 seconds. As a whole, the automatic AAA segmentation takes place in less than 3 seconds.

3.2 Lumen segmentation results

For the lumen segmentation stage, the parameters were set up by default with the following values:

- Fuzzyness membership exponent (*m*) (Eq. 1, 2 and 5): 2.
- Membership matrix exponent of the SFCM algorithm (*p*) (Eq. 4): 1
- Spatial function exponent of the SFCM algorithm (*q*) (Eq. 4): 1
- Area exponent in the lumen factor calculation (*r*) (Eq. 7): 1
- Circularity exponent in the lumen factor calculation (*s*) (Eq. 7): 1.5

Fig. 9 shows the results of the lumen segmentation using these parameters on a MR test image.

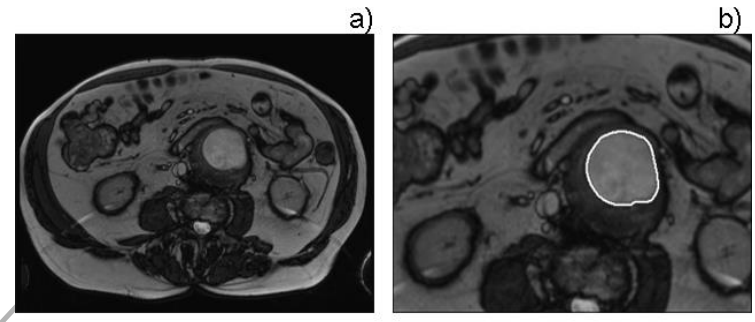

Fig. 9. Lumen segmentation stage results in our method. (a) Input MR image; (b) automatically segmented lumen contour.

The obtained lumen segmentation is correct in all the cases whenever the size of the lumen is big enough in relation to the size of the analyzed windowed image. Therefore, it is very important the selection of the region of interest accomplished in the pre-processing stage (see section 2). By reducing the area of interest around the aorta, the relative size of the lumen in relation to the size of the analyzed image increases,

providing the correct results in all the tested cases.

3.3 Aortic wall segmentation results

For the aortic wall segmentation stage, the parameters were set up by default with the following values:

- "Camera noise" factor (σ) (Eq. 9): 2
- Intensity gradient exponent (γ) (Eq. 9): 2
- Intensity-based parameter exponent (ρ) (Eq. 9): 2

To evaluate the results, the outer aortic boundary detected automatically through the proposed method was compared to the boundary validated by an expert. The performance of the method was measured by calculating the ratio of segmented boundary in our method that overlaps with the selection made by the expert. Fig. 10 shows a comparison between the automatic segmentation obtained by our method (Fig. 10a) and the expert validated segmentation (Fig. 10b) in one of the tested MR images.

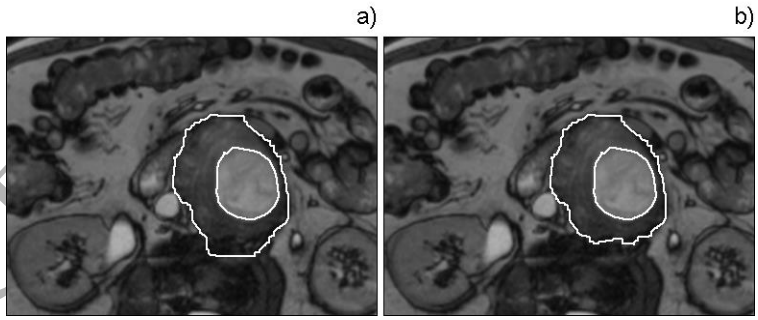

Fig. 10. Example of aortic segmentation in our method compared with an expert-validated segmentation. (a) Segmentation obtained automatically using our method; (b) segmentation by the expert.

In Table 1, we present the results of the automatic aortic wall segmentation stage for each patient. For the analyzed cases, the proposed method provides automatically

the aortic boundary segmentation, according to the expert criterion, with an average contour overlapping of the 79%.

TABLE I
AUTOMATIC AORTIC WALL SEGMENTATION RESULTS (% OF CORRECT CONTOUR SEGMENTED)

Test	Contour overlapping
Patient 1	82%
Patient 2	63%
Patient 3	45%
Patient 4	92%
Patient 5	70%
Patient 6	100 %
Patient 7	88%
Patient 8	89%
Average results	**79%**

It is important to note that these differences on the contour overlapping are a priori expected because the proposed method has been designed with a tendency to leak in the segmentation. Thus, the automatic segmentation tends to overestimate the aortic contour since it is more desirable to include surrounding tissues in conflictive areas and avoid cutting through aortic structures. In Fig. 10, we can see an example.

Among the causes of the leaking, the spinal area located under the aorta has proven to be error-prone for the method. The case presented in Fig. 10 is affected by this problem. The cause is the effect of the low intensity found in this area on the constraints used to define the cut. As there is no bright object adjacent to the aortic wall, the intensity gradient is lower and more difficult to detect. Moreover some intensity values in this area fall under the threshold of the intensity-based parameter, $\mu_{i,j}$, of the cost function (see Eq. 9) and attracts the cut.

Another cause for leakage is the presence of small objects outside the aortic contour. In the case of bright objects isolated from other abdominal structures, the method may include them inside the segmented contour. The cause of this problem is

either these objects being too small and being disregarded when the automatic graph cut initialization is generated or not being bright enough to appear in the SFCM algorithm results and therefore not appearing in the initialization.

4. Conclusion

AAA identification using image analysis can be of great help to doctors because they can be warned of an anomaly that could not be detected without a more specific study.. AAA diagnosis involves detection and segmentation of the lumen and the wall of the aorta in order to study whether there is an abnormal dilation of the aorta.

For this task, many procedures can be found in the literature, although they are usually semi-automatic processes that need the assistance of an expert, besides of presenting a high computational cost. Moreover, some of them fail when they are applied on MR images.

Thus, it becomes crucial to provide a solution that can constitute a real and automatic expert system for assisting doctors in the AAA diagnosis. In this sense, a novel methodology is presented in this work, which is performed through a complete automatic and low computational cost program. These features, along with a good accuracy in the analysis of MR images, constitute the high-impact points of the proposed procedure.

For that, the proposed scheme uses a combination of different techniques, profiting from their respective advantages and minimizing the corresponding drawbacks. Concretely, the developed AAA segmentation approach is divided in two different stages. In a first stage, the lumen is extracted using the SFCM algorithm and subsequently, in the second stage, the aortic wall is segmented using a graph-cut algorithm. To overcome the need of a manual initialization for the graph cut, the results

of the first stage are employed with the purpose of generating an automatic initialization (in addition to its original goal of lumen segmentation). In this way, we get an automatic method to segment the aortic wall with a low computational cost. The processing time of performing the whole AAA automatic segmentation takes less than 3 seconds.

Furthermore, the results have proven to be pretty successful. Assuming that the lumen is correctly segmented in the first stage, the automatic aortic wall segmentation is obtained with an average of 79% of the contour matching the contour validated by the expert for all the analyzed cases, which is a huge improvement over other existing methods where the complete graph cut initialization has to be done manually.

The differences in the contour between the automatic and the expert-validated results are caused by the estimation of a large undefined region in the graph cut initialization. Dark structures or bright objects of small size next to the aorta have proven to be problematic and to cause leaks in the segmented contour.

Thus, the developed method shows promising results. Furthermore, this combination can be used for the segmentation of other structures with similar problems in the medical area and also in other areas in which image analysis and segmentation is needed. It should also be noted that the presented results have been applied to single (2D) MR images. As a further expansion of the method, an adaptation to 3D sets of MR images (e.g. using a 6-neighborhood system for the graph cut stage) is likely to improve the results presented in this paper as more information becomes available to the algorithm.

Acknowledgments

We would like to thank to Dr. Sánchez from the “Ciudad Jardín” Health Center and Dr. Fernandez, from the Hospital of Torrevieja, their help in the medical context of the paper.

References

Ahmed, M.N., Yamany, S.M., Mohamed, N.A., Farag, A.A., 1999. A modified fuzzy c-means algorithm for MRI bias field estimation and adaptive segmentation. Medical Image Computing and Computer-Assisted Intervention, Miccai'99, Proceedings 1679, 72-81.

Ayyalasomayajula, A., Polk, A., Basudhar, A., Missoum, S., Nissim, L., Vande Geest, J.P., 2010. Three dimensional active contours for the reconstruction of abdominal aortic aneurysms. Annals of biomedical engineering 38, 164-176.

Borghi, A., Wood, N.B., Mohiaddin, R.H., Xu, X.Y., 2006. 3D geometric reconstruction of thoracic aortic aneurysms. Biomed Eng Online 5.

Boykov, Y., Kolmogorov, V., 2004. An experimental comparison of min-cut/max-flow algorithms for energy minimization in vision. Ieee T Pattern Anal 26, 1124-1137.

Boykov, Y., Veksler, O., Zabih, R., 2001. Fast approximate energy minimization via graph cuts. Ieee T Pattern Anal 23, 1222-1239.

Boykov, Y.Y., Jolly, M.P., 2001. Interactive graph cuts for optimal boundary & region segmentation of objects in N-D images. Eighth Ieee International Conference on Computer Vision, Vol I, Proceedings, 105-112.

Chuang, K.S., Tzeng, H.L., Chen, S., Wu, J., Chen, T.J., 2006. Fuzzy c-means clustering with spatial information for image segmentation. Comput Med Imag Grap 30, 9-15.

Duquette, A.A., Jodoin, P.M., Bouchot, O., Lalande, A., 2012. 3D segmentation of abdominal aorta from CT-scan and MR images. Comput Med Imag Grap 36, 294-303.

Freiman, M., Esses, S.J., Joskowicz, L., Sosna, J., 2010. An Iterative Model-Constrained Graph-Cut Algorithm for Abdominal Aortic Aneurysm Thrombus Segmentation. I S Biomed Imaging, 672-675.

Hameeteman, K., Rozie, S., Metz, C.T., Manniesing, R., van Walsum, T., van der Lugt, A., Niessen, W.J., Klein, S., 2013. Automatic carotid artery distensibility measurements from CTA using nonrigid registration. Medical image analysis 17, 515-524.

Haulon, S., Lions, C., McFadden, E.P., Koussa, M., Gaxotte, V., Halna, P., Beregi, J.P., 2001. Prospective evaluation of magnetic resonance imaging after endovascular treatment of infrarenal aortic aneurysms. European journal of vascular and endovascular surgery : the official journal of the European Society for Vascular Surgery 22, 62-69.

Hutchison, S.J., 2009. Aortic Diseases: Clinical Diagnosis Atlas, 1 ed.

Isselbacher, E.M., 2005. Thoracic and abdominal aortic aneurysms. Circulation 111, 816-828.

Kass, M., Witkin, A., Terzopoulos, D., 1988. Snakes: Active Contour Models. International Journal of Computer Vision, 321-331.

Kim, H.C., Park, S.W., Nam, K.W., Choi, H., Choir, E.J., Jig, S., Kim, M.G., Sun, K., 2010. Determination of accurate stent graft configuration in abdominal aortic aneurysm using computed tomography: a preliminary study. Clin Imag 34, 255-262.

Kronman, A., Joskowicz, L., 2015. A geometric method for the detection and correction of segmentation leaks of anatomical structures in volumetric medical images. International Journal of Computer Assisted Radiology and Surgery, 1-12.

Lee, K., Johnson, R.K., Yin, Y., Wahle, A., Olszewski, M.E., Scholz, T.D., Sonka, M., 2010. Three-dimensional thrombus segmentation in abdominal aortic aneurysms using graph search based on a triangular mesh. Computers in biology and medicine 40, 271-278.

Loncaric, S., Kovacevic, D., Sorantin, E., 2000. Semi-automatic active contour approach to segmentation of computed tomography volumes. P Soc Photo-Opt Ins 1, 917-924.

Lopez-Mir, F., Naranjo, V., Angulo, J., Villanueva, E., Alcaniz, M., Lopez-Celada, S., 2011. Aorta Segmentation Using the Watershed Algorithm for an Augmented Reality System in Laparoscopic Surgery. Ieee Image Proc.

Macia, I., Legarreta, J.H., Paloc, C., Grana, M., Maiora, J., Garcia, G., de Blas, M., 2009. Segmentation of Abdominal Aortic Aneurysms in CT Images Using a Radial Model Approach. Lect Notes Comput Sc 5788, 664-671.

Maiora, J., Ayerdi, B., Graña, M., 2014. Random forest active learning for AAA thrombus segmentation in computed tomography angiography images. Neurocomputing 126, 71-77.

Majd, E.M., Sheikh, U.U., Abu-Bakar, S.A.R., 2010. Automatic Segmentation of Abdominal Aortic Aneurysm in Computed Tomography Images Using Spatial Fuzzy C-Means, Sixth International Conference on Signal-Image Technology and Internet Based Systems, Kuala Lumpur, pp. 170-175.

Nakhjavanlo, B.B., Ellis, T.J., Soan, P.H., Dehmeshki, J., 2011. 3D Medical Image Segmentation Using Level Set Models and Anisotropic Diffusion, Seventh International Conference on Signal-Image Technology and Internet-Based Systems (SITIS). Dijon, pp. 403-408.

Pham, T.D., Golledge, J., 2008. Geostatistically Constrained Fuzzy Segmentation of Abdominal Aortic Aneurysm CT Images. Ieee Int Conf Fuzzy, 1448-1453.

Shang, E.K., Lai, E., Pouch, A.M., Hinmon, R., Gorman, R.C., Gorman, J.H., Sehgal, C.M., Ferrari, G., Bavaria, J.E., Jackson, B.M., 2015. Validation of semiautomated and locally resolved aortic wall thickness measurements from computed tomography. Journal of Vascular Surgery 61, 1034-1040.

Shim, M.B., Gunay, M., Shimada, K., 2009. Three-dimensional shape reconstruction of abdominal aortic aneurysm. Comput Aided Design 41, 555-565.

Soille, P., 1999. Morphological image analysis : principles and applications. Springer, Berlin [etc.].

Subasic, M., Loncaric, S., Sorantin, E., 2005. Model-based quantitative AAA image analysis using a priori knowledge. Comput Meth Prog Bio 80, 103-114.

Tauber, C., Batatia, H., Ayache, A., 2010. Quasi-automatic initialization for parametric active contours. Pattern Recogn Lett 31, 83-90.

Xu, C.Y., Prince, J.L., 1998. Snakes, shapes, and gradient vector flow. Ieee T Image Process 7, 359-369.

Zhao, F., Zhang, H., Wahle, A., Thomas, M.T., Stolpen, A.H., Scholz, T.D., Sonka, M., 2009. Congenital aortic disease: 4D magnetic resonance segmentation and quantitative analysis. Medical image analysis 13, 483-493.

Zohios, C., Kossioris, G., Papaharilaou, Y., 2012. Geometrical methods for level set based abdominal aortic aneurysm thrombus and outer wall 2D image segmentation. Comput Meth Prog Bio 107, 202-217.